

Diagnosing the energy cascade in a model of the North Atlantic

F. Schlösser and C. Eden

IFM-GEOMAR, Kiel, Germany

Spectral potential and kinetic energy densities and fluxes in horizontal wavenumber space are estimated in an eddy-resolving model of the North Atlantic. In agreement to recent observational results near surface kinetic energy fluxes are negative over wide regions of the North Atlantic, indicative of an inverse energy cascade. This inverse kinetic energy cascade is found over a wide depth range but both the spectral kinetic energy density and the corresponding flux show no clear dependency on Rossby radius or Rhines scale. Potential energy fluxes tend to be positive and show a direct potential energy cascade towards a scale which is related to the Rossby radius in the subtropical North Atlantic.

1. Introduction

Because of strong stratification and Earth' rotation, the large-scale atmospheric and oceanic flow is predominantly two-dimensional. An important feature of two-dimensional turbulent flow is the counterintuitive tendency of non-linear interactions to transfer energy from smaller to larger spatial scales [Kraichnan, 1967; Batchelor, 1969]. This is different from three-dimensional turbulent flow, in which the energy cascades from large to small scales where it is predominantly dissipated [Kolmogorov, 1941]. The direction of the energy cascades in the atmosphere and ocean and the scale at which energy dissipation is strongest, appears to be mandatory not just to understand the energy cycles in the atmosphere and the ocean, but also for a possible parameterisation of turbulent eddy fluxes, which is still missing (but urgently needed) for the ocean.

Based on idealised models of the atmosphere, it has been suggested [Salmon, 1998] that the depth independent (barotropic) flow indeed behaves as in two-dimensional turbulence, while the deviation (the baroclinic flow) shows an energy cascade to smaller scales. In this picture of the atmospheric energy cycle, the differential solar heating acts as a source of baroclinic energy on large scales, which cascades to smaller scales (i.e. the Rossby radius) where it is (partly) converted to barotropic energy, cascading again to larger scales, where it is dissipated, eventually by bottom friction.

For the ocean, on the other hand, the situation is less clear, since here, the barotropic flow is less dominant, topographic control can be much stronger and, furthermore, the lack of observations complicates the understanding of the oceanic energy cycle [Wunsch and Ferrari, 2004]. Using an idealised ocean model, Hua and Haidvogel [1986] reported that for a stratification as found in the ocean, with a sharp thermocline as its main characteristic, the atmospheric picture still remains valid with respect to the direction of the energy cascades. Smith [2001] found in a similar model that the presence of a shallow thermocline hampers the transfer of baroclinic to barotropic energy at the Rossby radius

compared to a model with stratification more similar to the atmosphere. Recently, Scott and Wang [2005] utilised the high spatial and temporal coverage of the turbulent oceanic flow in satellite altimeter data of the South Pacific Ocean, to calculate spectral kinetic energy fluxes from near surface geostrophic velocities and indeed found an (inverse) kinetic energy cascade towards larger scales, similar to corresponding results in the atmosphere [Boer, 1983].

In this paper, a realistic eddy-resolving model of the North Atlantic is used for similar calculations. Here, we are able to explore the direction of kinetic energy fluxes in the whole depth range and for the full velocities. In addition, we explore the available potential energy densities and corresponding fluxes in wavenumber space. The model characteristics, the data processing and the methodology to analyse the energy cascade are outlined in section 2. In section 3, we present the results of our calculations. A summary and discussion of these results is found in section 4

2. Model and methodology

The model which we use in this study is based on a rewritten version of MOM2 [Pacanowski, 1995] and identical to the one used e.g. in Eden et al. [2006]. The model domain covers the North Atlantic Ocean with horizontal resolution of $1/12^\circ$ and with 45 vertical levels. Simulated horizontal velocity, temperature and salinity used in the subsequent analysis are given every three days over a period of six years following the (10-yr) spinup period of the model.

Spectral potential and kinetic energy densities and corresponding fluxes in wavenumber space are estimated for several subregions of the model domain, each containing 150×150 data points, i.e. the resolved wavelengths, L (wavenumbers, $k = \frac{2\pi}{L}$), range from about $L = 8 \text{ km}$ ($k = 0.8 \text{ km}^{-1}$) to $L = 1200 \text{ km}$ ($k = 0.005 \text{ km}^{-1}$) at a nominal latitude of 30°N . The subregions are shown in Figure 1. Available potential energy (ϕ) is computed as $\phi = N^{-2} \frac{b^2}{2}$ (e.g. Salmon [1998]), where b denotes (potential) buoyancy (referenced to the sea surface) from which the horizontal mean buoyancy, $\langle b \rangle$, of each sub region has been removed. N^2 denotes the mean stratification given by $\frac{\partial}{\partial z} \langle b \rangle = N^2$. A two dimensional Fourier transformation is used in each subregion to obtain estimates of spectral densities of potential and kinetic energy. Furthermore, following Frisch [1995] and Scott and Wang [2005], high and low pass filtered versions of the velocities and potential densities are used to calculate the spectral kinetic energy flux Π_K

$$\Pi_K = \langle \mathbf{u}_K^< \cdot (\mathbf{u}_K^< \cdot \nabla \mathbf{u}_K^>) \rangle + \langle \mathbf{u}_K^< \cdot (\mathbf{u}_K^> \cdot \nabla \mathbf{u}_K^>) \rangle \quad (1)$$

and the spectral potential energy flux B_K

$$B_K = N^{-2} \langle b_K^< \mathbf{u}_K^< \cdot \nabla b_K^> \rangle + N^{-2} \langle b_K^< \mathbf{u}_K^> \cdot \nabla b_K^> \rangle \quad (2)$$

Here, $\mathbf{u}_K^<$ ($\mathbf{u}_K^>$) and $b_K^<$ ($b_K^>$) denote the lowpass (high-pass) filtered velocities and buoyancies, respectively, with respect to the cut-off wavenumber K , with $K = |\mathbf{k}|$ where \mathbf{k} denotes the horizontal wavenumber vector. The brackets $\langle \dots \rangle$ denote a horizontal average over each subregion shown in Figure 1. Note that the theoretical predictions concerning the energy flux direction refer to modal kinds of energy,

i.e. often to baroclinic and barotropic energies in a two-layer QG system. Although it was our aim to connect the results of the realistic North Atlantic model to the theoretical predictions, a meaningful modal decomposition is difficult (or even impossible) in the presence of strong topographic variations and changes in stratification. Here, we discuss the local or level form of energy instead. Although this diagnosis deviates somewhat from the theoretical suggestions, it stays close to the precursory study by Scott and Wang [2005].

For Π_K we have assumed horizontally non-divergent velocities. We have checked this assumption in the model and found only small changes, in agreement to quasi-geostrophic scaling. Double periodic boundary conditions are also assumed for each subregion. Certainly, this assumption resembles the major weakness of this approach. Note that Scott and Wang [2005] using the same assumption found little sensitivity of the results to the size of the (double periodic) boxes. Six years of model output are used for averaging the spectral energy fluxes and densities. In the subregions in the south-eastern North Atlantic, conditions are getting closest to isotropy as a prerequisite for the use of periodic boundary conditions, but in particular for the north-westernmost boxes strong mean currents can be expected and spatial inhomogeneities might influence the results. As in Scott and Wang [2005], a Hamming window is applied prior to the Fourier transformation. The method was tested by calculating energy fluxes without applying a Hamming window and by transforming the data on an $1/3^\circ$ grid before doing the calculations. The results were found to be slightly sensitive to these changes in both cases, but, however, main findings presented here remained the same.

We will discuss the spectral wavenumber densities and fluxes with respect to the Rossby radius L_r and the Rhines scale L_R . The Rossby radius is estimated from the time mean model stratification following Chelton et al. [1998] by calculating $L_r = \int_{-H}^0 \frac{N}{|f|\pi} dz$, shown in Figure 1 a). The variations of L_r are in the inner ocean to first order determined by the variation of the Coriolis parameter f and thus by latitude. The Rhines scale is calculated as $L_R = \left(\frac{u_{rms}}{\beta}\right)^{1/2}$ where the turbulent barotropic velocity scale u_{rms} denotes where $u_{rms}^2 = |\mathbf{u}_b - \bar{\mathbf{u}}_b|^2$ with $\mathbf{u}_b = |h^{-1} \int_{-h}^0 \mathbf{u} dz|$ and the temporal mean $\bar{\mathbf{u}}_b$. Although L_R , shown in Figure 1 b), depends on latitude via β , variations of u_{rms} dominate in L_R .

3. Results

3.1. Spectral energy density

Although the energy spectra vary horizontally and vertically, certain common features can be found in all areas of the North Atlantic being subject to this analysis. These features can be seen in Figure 2 for the mid box of the grid shown in Figure 1 centred at $31^\circ N$, $36^\circ W$. The mean spectral potential (red) and kinetic (blue) energy densities are shown on a double logarithmic scale. The kinetic energy is calculated at 50 m depth and potential energy at 500 m depth. From Figure 2, it is clear that the potential energy density is much larger than the kinetic energy on any scale under consideration, and that the difference between both energy forms is getting larger on largest scales. Note that the amplitude of kinetic energy density further decreases with depth, i.e. is always much less than the potential energy. While the kinetic energy density peaks around $0.02 km^{-1}$ ($L \approx 300 km$), the potential energy density shows no distinctive local maximum in the analysed spectral range. For comparison, the black lines show $k^{-5/3}$ and k^{-3} slopes. In the range of $k \approx 0.02 - 0.1 km^{-1}$ ($L \approx 60 - 300 km$) both spectra show slopes similar to k^{-3} .

3.2. Kinetic energy density and fluxes

In Figure 3 (left panels), the normalised spectral kinetic energy densities (dashed) and fluxes (solid) at 50m depth are shown for all nine subregions on a linear scale. The results are sorted both by latitude (upper, middle and lower picture) and by longitude (green - $48^\circ W$, black - $36^\circ W$ and blue - $24^\circ W$). The vertical lines denote the corresponding box-averaged Rhines scales (top) and Rossby radii (bottom). Note that all kinetic energy fluxes (and B_K) exactly go to zero for the wavenumber of the smallest resolved scale ($k \approx 0.8 km^{-1}$, $L \approx 8 km$). However, since fluxes and energy densities tend to vanish already for larger scales, only wavenumbers $k < 0.1 km^{-1}$ are shown. A negative kinetic energy flux is found in the high energy density range in all cases. A maximum (minimum) can be found in the spectral kinetic energy density (flux) around $k = 0.02 km^{-1}$ ($L \approx 300 km$), whereas the density maximum tend to show up at a slightly larger scale than the corresponding flux minimum. There is no first order dependence on parameters as such as the Rhines scale, L_R or Rossby radius, L_r , and in particular no apparent latitudinal dependency of the extrema in both the kinetic energy density and the flux.

To show their depth dependency, Figure 4 shows the normalised spectral kinetic energy densities (a) and spectral kinetic fluxes (b) for the subregion centred at $31^\circ N$, $36^\circ W$ at 50 (blue), 300 (green) and 500 (red) m depth. Although the amplitudes of the energy densities and fluxes decrease with depth (not shown), the location of the extrema of both the kinetic energy densities and fluxes vary little with depth and the fluxes remain negative throughout the water column. The only apparent depth dependency is given by decreasing kinetic energy densities and corresponding fluxes at larger wavenumbers ($L \approx 80 - 200 km$) for larger depths.

3.3. Potential energy density and fluxes

In Figure 3 (right panels), the normalised spectral potential energy densities (dashed) and the corresponding fluxes (solid) are shown for all nine subregions at 300 m depth. The results are again sorted both by latitude (upper, middle and lower picture) and by longitude (green - $48^\circ W$, black - $36^\circ W$ and blue - $24^\circ W$). The vertical lines denote the corresponding box-averaged Rhines scales (top) and Rossby radii (bottom). Note that the normalised potential energy spectra and fluxes at 500 m depth were found to be similar to Figure 3.

All potential energy spectra show a maximum at the smallest resolved wavenumber ($L \approx 1200 km$) and a more or less continuous decrease for larger wavenumbers, in contrast to the kinetic energy which shows a spectral peak at $L \approx 300 km$. Note that the maximum in the potential energy spectra still remains on the largest scale when we combine four boxes to a single one, in order to double the largest resolved wavelength.

Generally, in all subregions, the potential energy flux shows a (local) maximum at a scale, L_P , which varies apparently with latitude. The scale L_P is in general larger than the Rossby radius, L_r , but L_P is getting smaller with increasing latitude similar to L_r . For smaller (larger) wavenumbers than $k_P = \frac{2\pi}{L_P}$, the potential energy flux tends to decrease (increase) potential energy in this spectral range, leading to a downscale flux of potential energy, i.e. a direct potential energy cascade.

Note that for the northernmost subregions, there tends to be a local minimum in the flux for even smaller wavenumbers ($k \approx 0.01 km^{-1}$, $L \approx 500 km$) leading to an increase (decrease) of potential energy for $L > 500 km$ ($500 km < L <$

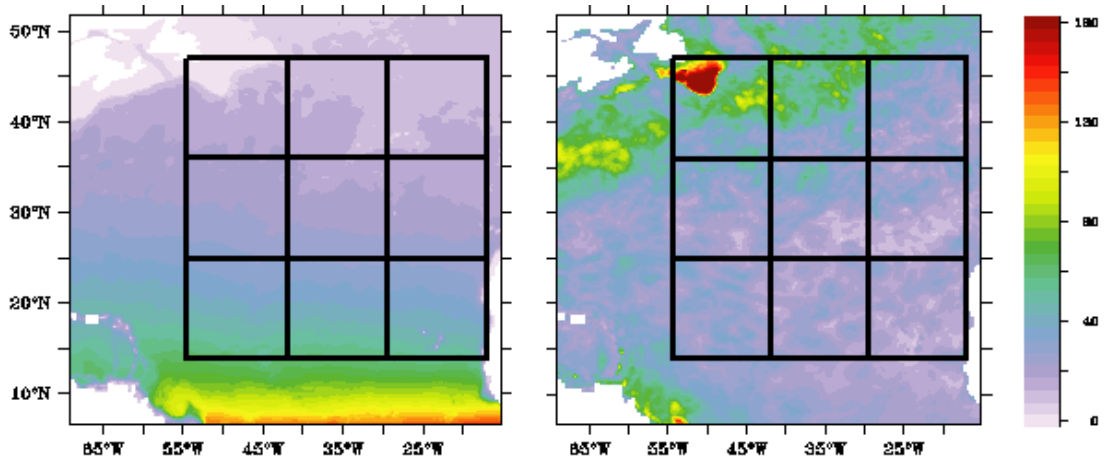


Figure 1. Left: First baroclinic Rossby radius, L_r , in km. Right: Rhines scale, L_R , in km. See text for definitions of L_r and L_R . The grid distinguishes the subregions for the spectral analysis.

L_P), pointing toward a possible further regime on larger scales with an inverse potential energy cascade up to the wavenumber k_P . The local minimum in the flux, however, does not show up in the southern subregions and might play therefore only a role for the subpolar regions of the ocean.

The potential energy fluxes vanish as k approaches the smallest resolved scales (not shown). However, they tend to be negative at the largest wavenumbers ($k = 0.1 \text{ km}^{-1}$, $L \approx 60 \text{ km}$) shown here. Note that this is in contrast to the kinetic energy fluxes which tend to converge to zero much faster for large wavenumbers. Note also that in principle, the boundary condition for all energy fluxes is zero flux at the largest and smallest resolved wavenumber and that in a quasi-stationary state an upscale energy flux at wavenumbers larger than $k = 0.1 \text{ km}^{-1}$ ($L \approx 60 \text{ km}$) is balanced by production of potential energy at smaller scales. However, this spectral range is certainly influenced by the subgrid-scale parameterisation in the model and consequently not further discussed here.

4. Summary and discussion

Spectral potential and kinetic energy densities and the corresponding energy fluxes have been estimated as a function of the horizontal wavenumber from an eddy-resolving North Atlantic model. Negative kinetic energy fluxes with a minimum at about $k = 0.02 \text{ km}^{-1}$ ($L \approx 300 \text{ km}$) have been found in all depth ranges and subregions considered here. This result is indicative of an inverse kinetic energy cascade from the mesoscale to the large scale and in agreement to the observational study by Scott and Wang [2005]. We find no significant regional modulations of the kinetic energy spectra or the spectral kinetic energy fluxes in the subtropical North Atlantic, in particular no clear dependency of extrema in kinetic energy density or flux on latitude, Rossby radius L_r or Rhines scale L_R .

Available potential energy does not show any spectral peak as the kinetic energy, but a continuous decrease from the largest to the smallest scales. Potential energy fluxes tend to be positive and downscale from the large scales to the mesoscale but there is also a negative flux of potential energy from the smallest scales to the mesoscales, which we have interpreted as influenced by subgrid-scale parameterisations of the model and/or artifacts of the analysis method.

The scale L_P , at which the potential energy flux peaks shows a strong latitudinal dependency. This is the scale at which the potential energy flux from the large scales is

largest and at which the reduction of potential energy by the energy flux due to the non-linear interactions by advective terms stops. Figure 5 shows the wavenumber of the maximal potential energy flux, $k_P = \frac{2\pi}{L_P}$, over the inverse of the box-averaged Rossby radius. The figure suggests a simple linear relationship between both, i.e. $L_P \approx 2\pi L_r$, which is approximately the scale at which baroclinic instability shows the largest growth rates in linear instability theory.

Note, however, that the spectral peak of the kinetic energy density or flux, shows no clear relationship on L_r (compare Figure 5). This is an important caveat since in a possible mixing parameterisation the relevant length scale for a mixing parameterisation, would be chosen near this peak in the kinetic energy spectrum. Our results suggests that this length scale could be chosen as a constant over wide regions of the North Atlantic.

Overall, our results confirm in parts the picture of the atmospheric energy cycle, given by e.g. Salmon [1998], and the ocean [Scott and Wang, 2005]. The kinetic energy shows an inverse energy cascade in which energy is transferred from the mesoscale to the largest scales at which it has to be dissipated (or converted to other energy forms). On the other hand, there is a direct energy cascade of potential, i.e. baroclinic energy from large to mesoscales.

Acknowledgments. FS is grateful to his parents and grandparents for financial support. Two reviewers helped to improve the manuscript. The model integrations have been performed on a NEX-SX8 at the University Kiel and on a NEC-SX6 at the Deutsches Klimarechenzentrum (DKRZ), Hamburg.

References

- Batchelor, G. K., 1969: Computation of the energy spectrum in homogeneous two-dimensional turbulence. *Phys. Fluids Suppl.*, **12B**, 233–239.
- Boer, G. J. and T. G. Shepherd, 1983: Large-scale two-dimensional turbulence in the atmosphere. *J. Atmos. Sci.*, **40**, 164–184.
- Chelton, D. B., R. A. deSzoeke, M. G. Schlax, K. E. Naggar, and N. Siwertz, 1998: Geographical variability of the first-baroclinic Rossby radius of deformation. *J. Phys. Oceanogr.*, **28**, 433–460.
- Eden, C., R. J. Greatbatch, and J. Willebrand, 2006: A diagnosis of thickness fluxes in an eddy-resolving model. *J. Phys. Oceanogr.*. In press.
- Frisch, U., 1995: *Turbulence: the Legacy of A.N. Kolmogorov*. Cambridge University Press, Cambridge, USA.

- Hua, B. L. and D. B. Haidvogel, 1986: Numerical simulations of the vertical structure of quasi-geostrophic turbulence. *J. Atmos. Sci.*, **43**, 2923–2936.
- Kolmogorov, A. N., 1941: Dissipation of energy in the locally isotropic turbulence (English translation). *Dokl. Akad. Nauk SSSR*, **32**, 19–21.
- Kraichnan, R. H., 1967: Inertial ranges in two-dimensional turbulence. *Phys. Fluids*, **10**, 1417–1423.
- Pacanowski, R. C., 1995: MOM 2 Documentation, User's Guide and Reference Manual. Technical report, GFDL Ocean Group, GFDL, Princeton, USA.
- Salmon, R., 1998: *Lectures on Geophysical Fluid Dynamics*. Oxford University Press, Oxford.
- Scott, R. B. and F. Wang, 2005: Direct evidence of an oceanic inverse kinetic energy cascade from satellite altimetry. *J. Phys. Oceanogr.*, **35**, 1650–1666.
- Smith, K. S. and G. K. Vallis, 2001: The scales and equilibration of midocean eddies: Freely evolving flow. *J. Phys. Oceanogr.*, **31**, 554–571.
- Wunsch, C. and R. Ferrari, 2004: Vertical mixing, energy and the general circulation of the oceans. *Annu. Rev. Fluid Mech.*, **36**, 281–314.

F. Schlösser, IFM-GEOMAR, FB I Ocean circulation and climate dynamics, Düsternbrooker Weg 20, 24105 Kiel, Germany. (fischloesser@ifm-geomar.de)

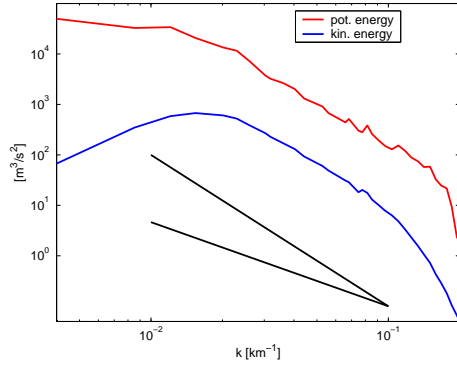


Figure 2. Spectral potential (red) and kinetic (blue) energy density in $m^3 s^{-2}$ for a subregion centred at $31^\circ N$, $36^\circ W$. Both spectral densities are shown on a double logarithmic scale. The black lines correspond to $k^{-5/3}$ and k^{-3} slopes.

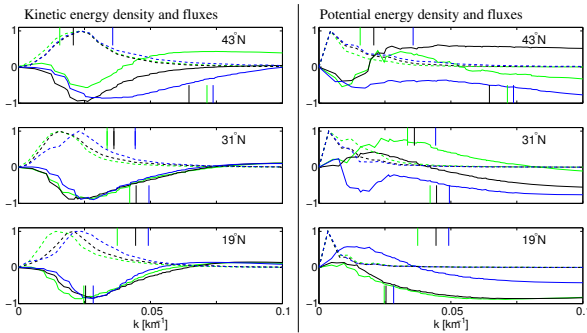


Figure 3. Left panels: Normalised spectral kinetic energy density (dashed) and normalised spectral kinetic energy flux (solid) at 50m depth at three different latitudes: $43^\circ N$ (top), $31^\circ N$ (middle) and $19^\circ N$ (bottom), the longitudes are $48^\circ W$ (green), $36^\circ W$ (black) and $24^\circ W$ (blue). Colored vertical lines denote the inverse box-averaged Rhines scale ($\langle L_R \rangle^{-1}$, top) and Rossby radius ($\langle L_r \rangle^{-1}$, bottom). Right panels: Same as left but for potential energy spectral densities and fluxes at 300m depth.

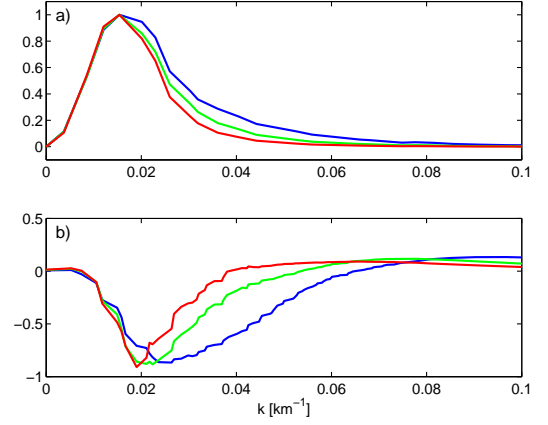


Figure 4. Normalised spectral kinetic energy density (a) and normalised spectral kinetic energy flux (b) in the subregion centred at $31^\circ N$, $36^\circ W$ in 50 (blue), 300 (green) and 500 (red) meters depth.

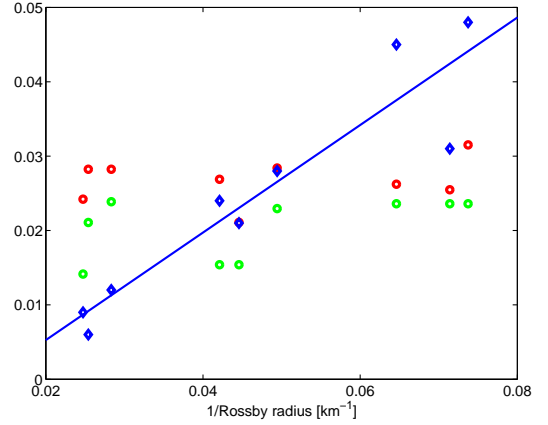


Figure 5. Blue diamonds: Local maximum of spectral potential energy flux, k_p , as shown in Figure 3, as a function of the corresponding inverse, box-averaged Rossby radius, $\langle L_r \rangle^{-1}$. Also shown is the regression between k_p vs. $\langle L_r \rangle^{-1}$, i.e. $k_p = 0.72 \langle L_r \rangle^{-1} - 0.01 \text{ km}^{-1}$ as the solid blue line. Green circles: Maximum of spectral kinetic energy density from Figure 3 vs. $\langle L_r \rangle^{-1}$. Red circles: Minimum of spectral kinetic energy fluxes vs. $\langle L_r \rangle^{-1}$.